ARTICLE

Exploring Advantages of Diverse Carbon Nanotube Forests with Tailored Structures Synthesized by Supergrowth from Engineered Catalysts

Bin Zhao,[†] Don N. Futaba,[†,*] Satoshi Yasuda,[†] Megumi Akoshima,[‡] Takeo Yamada,[†] and Kenji Hata[†,*]

[†]Nanotube Research Center, and [‡]Thermo Physical Properties Section, NMIJ, National Institute of Advanced Industrial Science and Technology (AIST), Tsukuba, Ibaraki, 305-8565, Japan

ABSTRACT We explored advantages of diverse carbon nanotube forests with tailored structures synthesized by water-assisted chemical vapor deposition (CVD) growth (supergrowth) from engineered catalysts. By controlling the catalyst film thickness, we synthesized carbon nanotube (CNT) forests composed from nanotubes with different size and wall number. With extensive characterizations, many interesting dependencies among CNT forest structures and their properties, which were unknown previously, were found. For example, multiwalled carbon nanotubes (MWNTs) showed superior electronic conductivity while single-walled carbon nanotubes (SWNTs) showed superior thermal diffusivity, and sparse MWNTs achieved lower threshold voltage for field emission than dense SWNTs. These interesting trends highlight the complexity in designing and choosing the optimum CNT forest for use in applications.

KEYWORDS: carbon nanotube, CNT · forest · single-walled carbon nanotube, SWNT · double-walled carbon nanotube, DWNT · multiwalled carbon nanotube, MWNT · hydrophobicity · structure · field emission · thermal diffusivity

When carbon nanotubes (CNTs) are efficiently grown by chemical vapor deposition (CVD) from catalysts deposited on a substrate, the subsequently grown CNTs align vertically into a bulk material ("CNT forest").[1−6] Possessing this unique structure, CNT forests are well established to be advantageous for numerous applications spanning from supercapacitors[7,8] and sensing applications[9] to field-emitters in flat-screen displays,[3] thermal interface materials,[10] electrical interconnects in nanoscale devices,[11] and superhydrophobic surfaces for self-cleaning surfaces.[12] This assorted utility of the CNT forest stems from alignment of nanotubes which preserves much of the one-dimensional nature of individual CNTs. As a result, forests exhibit promising electronic and thermal conductivity, field emission property, hydrophobicity, high carbon purity, and high surface area.

To extract the full potential of CNT forests, it is important to tailor these properties to meet the demands of the target application. Achieving this goal requires the ability to tailor not only one but several properties. For example, for supercapacitor applications, high surface area is required for high energy density; high purity is needed for long lifetime, and alignment and good electronic conductivity are needed for high power. Tailoring several properties is not straightforward, since in many cases, the key properties are interdependent and cannot be controlled independently. Tailoring the structure of the forest is the most promising approach to tailor the properties. For example, to achieve low threshold electron field emission, the nanotube radius of curvature (tube diameter) and spacing between nanotubes are critical to increase the local electric field and avoid intertube screening effects, respectively. The forest structure includes both the individual nanotubes and how they are assembled. The individual nanotubes can vary in diameter, wall number, and length, and these nanotubes can be assembled with different spacing. As such, the key to unlock the full potential of CNT forests is to understand how forest properties depend on its structures.

The structure of the forest depends on the sample preparation and synthesis conditions. Having a straightforward approach to control the structure of the forests would be advantageous, so that it is both reproducible and easily controllable. One powerful approach to control the structure of the forest is to engineer the catalyst through controlling the thickness of the catalytic thin metal film.[2] A thin metal film is widely used as a standard catalyst for CNT forest

*Address correspondence to kenji-hata@aist.go.jp, d-futaba@aist.go.jp.

Received for review October 3, 2008 and accepted December 10, 2008.

Published online December 22, 2008. 10.1021/nn800648a CCC: $40.75

growth. When this film is annealed, it converts into well-isolated, individual nanoparticles which act as catalysts for nanotube growth.[13,14] Empirically it is known that an increase in the Fe film thickness increases the average catalyst size and the average nanotube diameter, and this phenomenon has been used to selectively synthesize double-walled carbon nanotube (DWNT) forests.[2,15,16]

In this paper, we have synthesized single-walled carbon nanotube (SWNT), DWNT, and multi-walled carbon nanotube (MWNT) forests and have performed an extensive survey of the structures and properties to explore the advantages of each type of carbon nanotube forests. Specifically, we grew a variety of CNT forests by water-assisted thermal CVD[1] ("supergrowth") from engineered catalysts.[2] By controlling the catalyst film thickness, we synthesized CNT forests composed from nanotubes with different sizes and wall number[2] and characterized their structures and properties. The main interesting findings were (i) the inverse relationship between the diameter (wall number) and intertube spacing of the nanotubes within a forest; (ii) the intrinsic higher growth efficiency of SWNT over MWNT forests; (iii) superior electronic conductivity of MWNTs over SWNTs; (iv) a decrease of thermal diffusivity of MWNT over SWNT forests; (v) a strong decrease of the specific surface area for MWNTs; and (vi) lower field-emission threshold voltage for MWNT forests. These interesting trends highlight the complexity in designing and choosing the optimum CNT forest for use in applications.

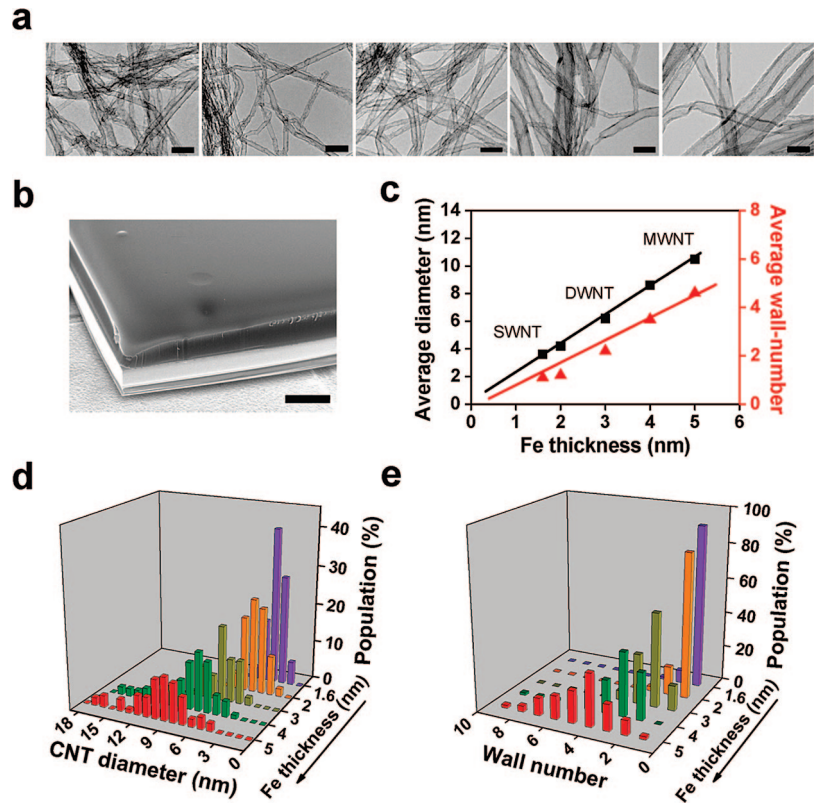

Figure 1. Characteristics of CNTs grown from Fe catalytic films of 1.6−5 nm. (a) TEM images of CNTs. Scale bar, 25 nm. (b) Scanning electron microscope image of a typical CNT forest. Scale bar, 1 mm. (c) Average diameter and wall-number as a function of Fe film thickness. (d) A histogram of CNT diameter distribution with Fe film thickness. (e) A histogram of wall-number distribution with Fe film thickness.

RESULTS AND DISCUSSION

To have the catalyst film thickness as the only control parameter, a single growth process was used. We searched for an optimal combination of catalyst composition, substrate, and growth conditions to grow the widest variety of forests with high efficiency with one growth process. We employed water-assisted thermal CVD ("supergrowth") with acetylene as the carbon source since this approach has the best growth efficiency enabling synthesis of high purity forests with millimeter scale in 10 min.[1] As summarized (Supporting Information Table T1), we investigated the 36 combinations of catalyst composition (Ni, Co, and Fe), catalyst thickness (2 and 4 nm), support layer (with and without Al_2O_3), and substrate (Ni and Fe metal foils, and Si). The Fe catalyst with Al_2O_3 support layer showed the best growth efficiency, followed by Ni catalyst with Al_2O_3 support. It is noteworthy that Ni is a commonly used catalyst for CNT growth in plasma-enhanced CVD; however, this extensive survey showed that Fe possesses superior growth efficiency for thermal CVD. For the Fe catalyst with Al_2O_3 support, we could grow forests (Figure 1b) of 500−1000 μm in height in a 10 min growth time with Fe catalyst films with a thickness in the range of 1.6−5 nm. Beyond the thickness of 5 nm, reproducibility and growth efficiency dropped dramatically.

First, we characterized individual nanotubes within the forests grown from Fe catalyst films with thickness in the range of 1.6−5 nm. Transmission electron microscopy (TEM) images (Figure 1a) showed that nanotubes became larger as catalyst film thickness increased. Interestingly, the average diameter and wall number increased linearly with film thickness (Figure 1c). The nanotubes grown from Fe layers of 1.6, 3, and 5 nm corresponded to SWNTs, DWNTs, and small MWNTs, respectively. A histogram of the diameter and wall number (Figure 1d,e) showed that both distributions broadened with increasing Fe thickness, evidenced by the 2.5/3 times increase in the fwhm, respectively.

Second, we characterized how individual nanotubes are assembled and found that forests composed from small/large nanotubes were dense/sparse. Specifically, the mass density of CNT forests monotonically decreased from 0.026 to 0.01 g/cm^3, the calculated nanotube spacing increased from 21 to 109 nm, and the volume occupancy[17,18] dropped from 2.7 to 0.8% with increased catalyst thickness (Figure 2a). Importantly,

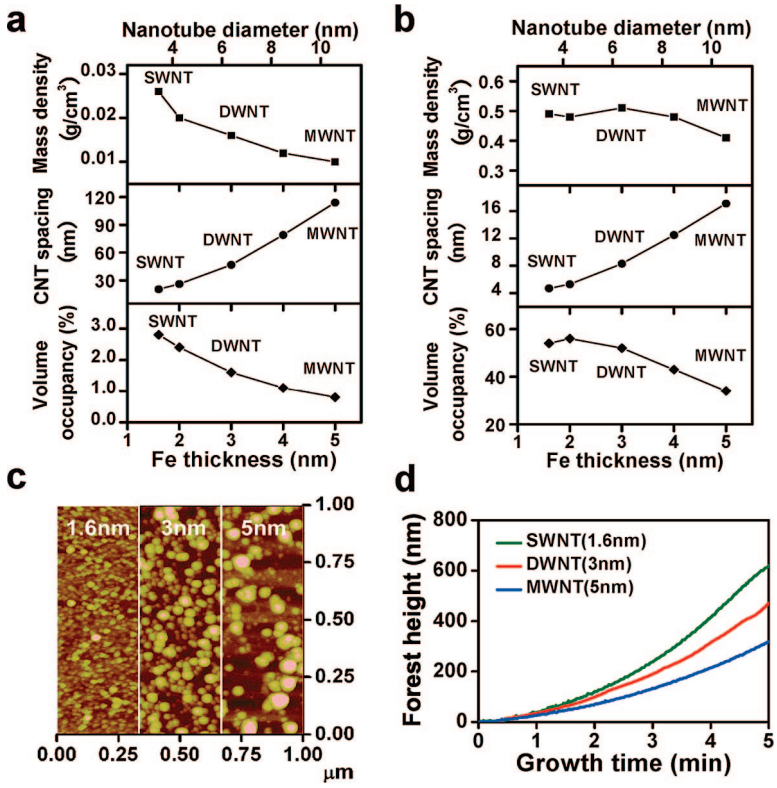

Figure 2. (a) Structural characteristics of CNT forests as a function of nanotube diameter and Fe film thickness; (b) structural characteristics of CNT solid as a function of nanotube diameter and Fe film thickness; (c) AFM images of Fe catalyst nanoparticles on Si substrates prior to growth process; (d) growth curves for SWNT, DWNT, and MWNT forests grown from 1.6, 3, and 5 nm, respectively.

these findings mean that the nanotube diameter and intertube spacing cannot be tailored independently, which imposes a fundamental restriction to what extent the structures of forests can be controlled within the framework of thin film catalytic system. All of these results are explainable from the nature of individual catalytic nanoparticle formation from thin catalytic films. It is well-known that thin/thick catalytic films break into small/large catalytic nanoparticles that produce small/large nanotubes. Here, as seen in the AFM images (Figure 2c), we additionally found that thin/thick catalytic films break into high/low density nanoparticles, which generate the inverse relationship between the diameter (wall number) and intertube spacing of the nanotubes within a forest.

The growth curves of forests (Figure 2d) were measured by an *in situ* telecentric height monitoring system. This system is our standard characterization tool for *in situ*, real-time height monitoring of nanotube forests which detects the projected shadow of the forest created from an parallel green light flow which is refocused onto a CCD through a telecentric optical system.[19] It was revealed that the growth rate decreased steadily from 125 to 65 μm/min as the wall number increased. This decrease in both the growth rate and density with wall number means that the growth efficiency (rate of graphitic wall growth) also decreases (~5.2 times) with wall number. We believe that this difference in growth rate stems directly from the difference in required carbon per unit length of a nanotube (*i.e.*, SWNTs intrinsically require less carbon per unit length; therefore, their growth rate is higher than that for larger diameter, multishelled tubes.) In contrast to conventional belief, these results demonstrate that SWNTs grow more efficiently than MWNTs within the framework of a thin film catalytic system.

The intertube spacing can be altered by post-growth processes such as liquid-induced solidification while retaining the nanotube diameter. When liquids are introduced into the forests and dried, the sparsely assembled nanotubes in the forests densely pack into a form called a nanotube solid.[18] This nanotube solid facilitates the measurement of certain physical properties not easily measured on the sparse CNT forest. Interestingly, the nanotube solid mass densities were surprisingly similar (*ca.* 0.47 g/cm^3) regardless of the wall number and initial forest mass densities (0.026−0.01 g/cm^3). With increased wall number, the intertube spacing increased monotonically while the volume occupancy decreased steadily (Figure 2b). These results indicate more disordered nanotube packing as the wall number increases, which we believe arises from an increase in tube stiffness and broadening in diameter distributions. The structural characterizations are summarized in Supporting Information Table T2 and Table T3.

To elucidate the advantages of each forest type, we investigated a number of properties of the forests spanning electronic and thermal conductivity, field emission, wettability, specific surface area, purity, and crystallinity. To begin, Raman spectroscopy and thermogravimetric analysis (TGA) were implemented to evaluate the degree of crystallinity and purity. Macro-Raman (532-nm wavelength) showed a decrease in the G-band intensity for forests of increased wall number, and thus the ratio between the G-band and D-band intensity (G/D ratio) decreased (Figure 3a). The radial breathing mode peaks (RBM), being an indicator of the existence of SWNTs, were most prominent for forests grown from thinner films and this is consistent with the TEM observations. TGA (Figure 3b,c) at ramp rate 2 °C/min in air showed no measurable residue remaining above 750 °C, indicating very high carbon purity. The combustion ranges of the forests were 550−680 °C with the peak weight reduction at about 640 °C. MWNT forests exhibited this peak at slightly lower temperatures. This and the Raman data consistently imply that nanotube with increased wall number have inferior crystallinity.[20,21]

CNT forests possess a very high specific surface area because nanotubes are not heavily bundled allowing efficient gas intercalation. Brunauer−Emmett−Teller (BET) surface areas[22] of the forests (40 mg) were estimated from nitrogen adsorption isotherms as 1250 ± 50, 750 ± 40, and 360 ± 20 m^2/g for SWNT, DWNT, and MWNT forests, respectively (Figure 3d). The α_s-plot, which is a comparison of the experimental adsorption data with a ideal infinite flat surface, determines the deviation of the surface area from the external surface area.[23] The good linearity in the range of $\alpha_s = 0.5 \sim 1.5$ (Supporting Information Figure S1) indicates that the nanotubes are closed and the nanotube inner surfaces were not exposed.[24] This result matches (Figure 3e) extremely well with the theoretical calculation by Peigney *et al.*,[25] where they concluded that the predominant factor which decreases the surface area of clean CNTs was wall number. Clearly forests grown from thin films are the choice for energy and material storage applications such as gas sensors and supercapacitors where surface area is the key property.

Recently, wettability of forests has attracted much attention because the surfaces of forests have been reported to show superhydrophobicity.[12] Here, we studied water wettability (Figure 3f) on forests by measuring the static contact angle (CA) and found that the CA increased from 100° to 120° and to 150° for SWNT, DWNT, and MWNT forests, respectively. We believe that this results from the increased spacing (therefore roughness) and diameter (lower surface energy) of the MWNT forest.[26] The combination of appropriate spacing and diameter allows for the superhydrophobic support of a water droplet for the case of MWNTs. Thus, MWNT forests are the choice for applications requiring the self-cleaning property, or so-called "Lotus effect",[27] of superhydrophobic micronanostructured surfaces.

Electronic conductivity is one of the most fundamental properties of nanotubes and here was examined by four-point resistance measurements on a 1 cm × 1 cm solid sheet made from a forest. Figure 4a shows that the electrical conductivity increased 2-fold with forests possessing increased wall number where the highest electrical conductivity of 125 S/cm (5 nm thick film), which is comparable to the state-of-the-art mixed-oxide spinel $Ni_xCo_{x-1}O_{3/4}$ (300 S/cm).[28] This trend stems from the fact that MWNT forests are composed mainly from metallic few-walled carbon nanotubes while SWNT forests include a large population of semiconductive single-walled carbon nanotubes. The electronic anisotropy is not as high as expected and requires future work to clarify. Summarizing, MWNT forests are the choice for applications requiring high electronic conductivity.

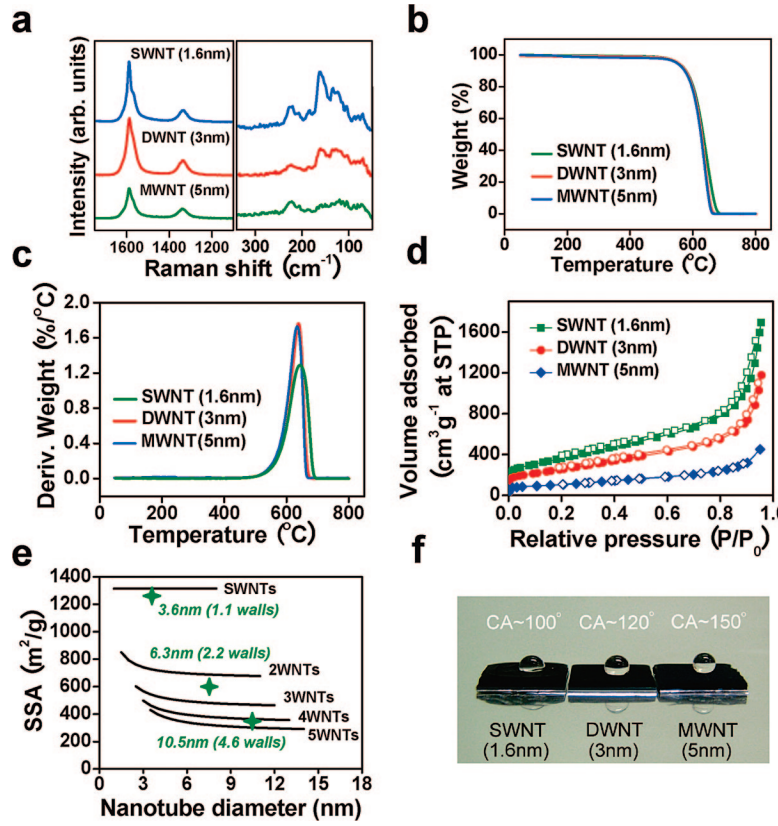

Figure 3. Physical properties of CNT forests grown from different Fe film thickness: (a) Raman spectra showing tangential mode (left) and radial breath mode (right) peaks; (b) TGA profile for different CNT samples; (c) TGA plot of the derivative weight as a function of the temperature; (d) adsorption (filled) and desorption (open) isotherms for N_2 at 77 K; (e) calculated specific surface area (SSA) of CNTs *versus* their diameter and wall number[25] (black lines) and experimentally measured BET-SSA for various CNT samples; (f) photograph of the static contact angle on SWNT, DWNT, and MWNT forests.

Thermal conductivity is another fundamental property of nanotubes, and here the thermal diffusivity was measured by the laser flash method[29] at room temperature on forests with a fixed height (~450 μm) to avoid any possible influence from height. Briefly, the thermal diffusivity is the ratio of thermal conductivity to volumetric heat capacity and is determined from the time required for the heat caused by a laser-generated light pulse to propagate across the sample. In sharp contrast to the case of electronic conductivity, we found that the thermal diffusivity values (Figure 4b) of CNT forests decreased 2-fold with increased wall number. Though these values are lower than isotropic graphite (1.0×10^{-4} m^2/s), it is superior to nickel (2×10^{-5} m^2/s) and sapphire (1.6×10^{-5} m^2/s). Unlike electronic conductivity where the semiconductive/metallic nature of the nanotube is important, thermal conductivity does not rely upon electron transport as heat is transferred predominantly by phonons in this temperature regime.[30] In general, phonon transport is more sensitive to defects than electron transport, and thus we interpret that inferior crystallinity of MWNTs causes this trend. These data thus conclude, in contrast to electronic conductiv-

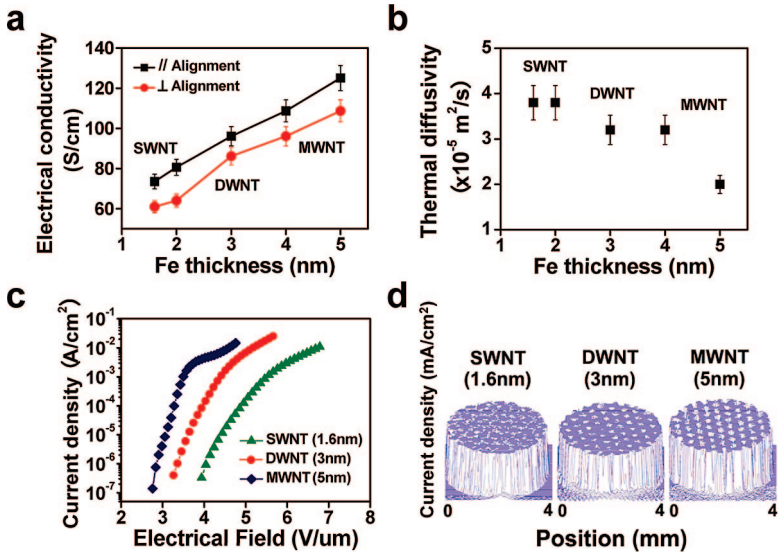

Figure 4. (a) Electrical conductivity of CNT solid sheets both parallel (black) and perpendicular (red) to alignment direction; (b) thermal diffusivity of CNT forests as a function of Fe film thickness; (c) emission current density as a function of applied electrical field for different CNT forests; (d) spatial mapping of the emission current at the range of 0.00−1.00 mA/cm^2 from different forests.

ity, SWNT forests are the choice for applications requiring high thermal diffusivity.

One important property of CNT forests is electron field emission. To avoid any possible influence by height, forests with a fixed height of ~40 μm were grown directly onto a conducting metal foil (YEF 426: (Fe−42%Ni−6%Cr)).[31] A grid-shaped mask was utilized to pattern the catalysts during sputtering in order to demonstrate spatial mapping of emission current clearly. Field emission current increased with increasing electric field following the Fowler−Nordheim (F−N) model (Supporting Information Figure S2), which describes the emission of electrons as a quantum mechanical tunneling process across the surface potential barrier under the influence of an electric field in difference with thermionic emission or photoemission.[32] Forests of nanotubes with large wall number exhibited lower threshold voltages (Figure 4c). To achieve a low threshold voltage, a forest of small diameter nanotubes with large intertube spacing (~2-times the height) would be ideal.[33] However, this situation is not easily achievable, as nanotube diameter and intertube spacing are in competition. In this case, the intertube spacing appeared dominant because the threshold voltage decreased despite increasing diameter (Figure 4c). This means that intertube screening effects, that reduce the local electric field, are more dominant than the diameter on the resulting threshold voltage. Three-dimensional spatial mappings of the electron emission current were generated from the lateral spatial mapping ($x-y$ axis) with a resolution of 10 μm and emission current at the range of 0.00−1.00 mA/cm^2 (z-axis) (Figure 4d) showing excellent homogeneity for all forests, which is important for display applications. The regular patterns observed in the emission mappings follow exactly the patterned CNT growth from masking. The field enhancement factor was estimated from the slope of experimental data to the F−N equation:[32]

$$I \propto \beta^2 V^2 / (d^2 \phi) \exp(B\phi^{3/2} d / \beta V)$$

in which I is the emission current, β is field enhancement factor, V is the applied voltage, ϕ is the work function, d is the interelectrode distance, and B is a constant (6.83×10^9 V eV$^{-3/2}$ m^{-1}). The field enhancement factors were estimated to be 790, 876, and 916 for SWNT, DWNT, and MWNT forests, respectively, which was consistent with the trend in the threshold voltages. Also, our results were comparable to those reported in literature,[34,35] indicating further improvements can be envisioned by controlling other parameters in addition to the catalytic film thickness. On the basis of our result, sparse MWNT forests are the choice for field emission applications within the framework of thin film catalytic system.

CONCLUSIONS

In conclusion, we synthesized a variety of carbon nanotube forests with tailored structures using supergrowth and engineered catalysts. By controlling only one key parameter, that is, the catalyst film thickness, we were able to synthesize diverse CNT forests composed from nanotubes with different diameter and wall number. We characterized their structures and properties and found many interesting dependencies among the properties and the structures previously unknown. For example, MWNTs showed superior electronic conductivity while SWNTs showed superior thermal diffusivity. These results clearly demonstrate the importance of appropriately linking the properties and structures of CNT forests to enable one to choose the best forest suited for the target application.

EXPERIMENTAL METHODS

Carbon nanotube (CNT) forests were synthesized in a 3-in. tube furnace by water-assisted chemical vapor deposition[1] with a diluted acetylene carbon source (10% acetylene + 90% He). Thin Al_2O_3 (~40 nm)/Fe (1.6−5.0 nm) metal layers sputtered on Si substrates with an oxidized layer of thickness 500 nm were used in all cases except field-emission samples. Water vapor was employed as a catalyst preserver and enhancer,[1,17,36] and was supplied by passing a portion of the helium carrier gas through a water bubbler. Pure helium (99.9999%) with hydrogen (99.99999%) (total flow 1000 cm^3 STP per minute) was used as a carrier gas at one atmosphere with a small and controlled amount of water vapor supplied from the water bubbler. Typical CVD growth was carried out at 780−810 °C with acetylene (30−50 cm^3 STP per minute) and a water concentration of 100−200 ppm for 10 min. The optimum water−carbon balance

depended significantly on experimental conditions, such as growth temperature, acetylene flow rate, catalyst, and the furnace.

CNT solid sheet was made from an as-grown forest by sandwiching the forest between two glass slides and pushing over the vertically aligned CNTs and then densifying them with capillary force of liquid.[18]

Transmission electron microscopy (TEM) images were taken using a Hitachi H-9000NA transmission electron microscope. Raman spectroscopy was performed using a thermo-electron Raman spectrometer with 532-nm excitation wavelength. Thermogravimetric analysis (TGA) was carried out using a TGA Q5000 analyzer (TA instruments). Samples were analyzed in platinum pans at a heating rate of 2 °C/min to 800 °C in 10 sccm (cm^3 STP per min) air flow. BET surface areas were estimated from nitrogen adsorption isotherms at 77 K for 40 mg nanotube samples using a BEL Japan: BELSORP Mini II surface-area and pore-size analysis system. Field-emission measurement were implemented using a cathode emission profiler (Tokyo Catholde Laboratory, CEPS-NW) with an anode−cathode distance of 300 μm and a scan area of 0.4 cm × 0.4 cm. Thermal measurement was performed in air under ambient temperature by a laser flash method.[29]

We estimated nanotube spacing and volume occupancy using CNT area density. From average diameter and wall-number, we could get average linear density of a nanotube, which is defined as the average mass of a CNT per unit length.[17] Then, CNT area density in a forest was calculated from mass density and linear density.

Acknowledgment. We are grateful for partial support by the Research and Development of Nanodevices for Practical Utilization of Nanotechnology Project of the New Energy and Industrial Technolgoy Development Organization (NEDO).

Supporting Information Available: Detailed survey results on combinations of catalyst composition, catalyst thickness, support layer, and substrate; structural characteristics of as-grown forests and CNT solids; α_s plot of BET measurement; F−N plot of field-emission measurement. This material is available free of charge via the Internet at http://pubs.acs.org.

REFERENCES AND NOTES

1. Hata, K.; Futaba, D. N.; Mizuno, K.; Namai, T.; Yumura, M.; Iijima, S. Water-Assisted Highly Efficient Synthesis of Impurity-Free Single-Walled Carbon Nanotubes. *Science* **2004**, *306*, 1362–1364.
2. Yamada, T.; Namai, T.; Hata, K.; Futaba, D. N.; Mizuno, K.; Fan, J.; Yudasaka, M.; Yumura, M.; Iijima, S. Size-Selective Growth of Double-Walled Carbon Nanotube Forests from Engineered Iron Catalysts. *Nat. Nanotechnol.* **2006**, *1*, 131–136.
3. Fan, S. S.; Chapline, M. G.; Franklin, N. R.; Tombler, T. W.; Cassell, A. M.; Dai, H. J. Self-Oriented Regular Arrays of Carbon Nanotubes and Their Field Emission Properties. *Science* **1999**, *283*, 512–514.
4. Wei, B. Q.; Vajtai, R.; Jung, Y.; Ward, J.; Zhang, R.; Ramanath, G.; Ajayan, P. M. Organized Assembly of Carbon Nanotubes. *Nature* **2002**, *416*, 495–496.
5. Murakami, Y.; Chiashi, S.; Miyauchi, Y.; Hu, M.; Ogura, M.; Okubo, M.; Maruyama, S. Growth of Vertically Aligned Single-Walled Carbon Nanotube Films on Quartz Substrates and Their Optical Anisotropy. *Chem. Phys. Lett.* **2004**, *385*, 298–303.
6. Zhong, G. F.; Iwasaki, T.; Robertson, J.; Kawarada, H. Growth Kinetics of 0.5 cm Vertically Aligned Single-Walled Carbon Nanotubes. *J. Phys. Chem. B* **2007**, *111*, 1907–1910.
7. Niu, C. M.; Sichel, E. K.; Hoch, R.; Moy, D.; Tennent, H. High Power Electrochemical Capacitors Based on Carbon Nanotube Electrodes. *Appl. Phys. Lett.* **1997**, *70*, 1480–1482.
8. Zhang, H.; Cao, G. P.; Yang, Y. S.; Gu, Z. N. Comparison Between Electrochemical Properties of Aligned Carbon Nanotube Array and Entangled Carbon Nanotube Electrodes. *J. Electrochem. Soc.* **2008**, *155*, K19−K22.
9. Li, J.; Ng, H. T.; Cassell, A.; Fan, W.; Chen, H.; Ye, Q.; Koehne, J.; Han, J.; Meyyappan, M. Carbon Nanotube Nanoelectrode Array for Ultrasensitive DNA Detection. *Nano Lett.* **2003**, *3*, 597–602.
10. Huang, H.; Liu, C. H.; Wu, Y.; Fan, S. S. Aligned Carbon Nanotube Composite Films for Thermal Management. *Adv. Mater.* **2005**, *17*, 1652–1656.
11. Li, J.; Ye, Q.; Cassell, A.; Ng, H. T.; Stevens, R.; Han, J.; Meyyappan, M. Bottom-up Approach for Carbon Nanotube Interconnects. *Appl. Phys. Lett.* **2003**, *82*, 2491–2493.
12. Lau, K. K. S.; Bico, J.; Teo, K. B. K.; Chhowalla, M.; Amaratunga, G. A. J.; Milne, W. I.; McKinley, G. H.; Gleason, K. K. Superhydrophobic Carbon Nanotube Forests. *Nano Lett.* **2003**, *3*, 1701–1705.
13. Seidel, R.; Liebau, M.; Duesberg, G. S.; Kreupl, F.; Unger, E.; Graham, A. P.; Hoenlein, W.; Pompe, W. In-Situ Contacted Single-Walled Carbon Nanotubes and Contact Improvement by Electroless Deposition. *Nano Lett.* **2003**, *3*, 965–968.
14. Zhang, R. Y.; Amlani, I.; Baker, J.; Tresek, J.; Tsui, R. K. Chemical Vapor Deposition of Single-Walled Carbon Nanotubes Using Ultrathin Ni/Al Film as Catalyst. *Nano Lett.* **2003**, *3*, 731–735.
15. Ci, L. J.; Vajtai, R.; Ajayan, P. M. Vertically Aligned Large-Diameter Double-Walled Carbon Nanotube Arrays Having Ultralow Density. *J. Phys. Chem. C* **2007**, *111*, 9077–9080.
16. Patole, S. P.; Alegaonkar, P. S.; Shin, H. C.; Yoo, J. B. Alignment and Wall Control of Ultra Long Carbon Nanotubes in Water Assisted Chemical Vapour Deposition. *J. Phys. D: Appl. Phys.* **2008**, *41*, 155311−1−155311−6.
17. Futaba, D. N.; Hata, K.; Namai, T.; Yamada, T.; Mizuno, K.; Hayamizu, Y.; Yumura, M.; Iijima, S. 84% Catalyst Activity of Water-Assisted Growth of Single Walled Carbon Nanotube Forest Characterization by a Statistical and Macroscopic Approach. *J. Phys. Chem. B* **2006**, *110*, 8035–8038.
18. Futaba, D. N.; Hata, K.; Yamda, T.; Hiraoka, T.; Hayamizu, Y.; Kakudate, Y.; Tanaike, O.; Hatori, H.; Yumura, M.; Iijima, S. Shape-Engineerable and High-Densely Packed Single-Walled Carbon Nanotubes. *Nat. Mater.* **2006**, *5*, 987–994.
19. Yasuda, S.; Futaba, D. N.; Yumura, M.; Iijima, S.; Hata, K. Diagnostics and Growth Control of Single-Walled Carbon Nanotube Forests Using a Telecentric Optical System For in-situ Height Monitoring. *App. Phys. Lett.* **2008**, *93*, 143115-1–143115-3.
20. McKee, G. S. B.; Vecchio, K. S. Thermogravimetric Analysis of Synthesis Variation Effects on CVD Generated Multiwalled Carbon Nanotubes. *J. Phys. Chem. B* **2006**, *110*, 1179–1186.
21. Bom, D.; Andrews, R.; Jacques, D.; Anthony, J.; Chen, B. L.; Meier, M. S.; Selegue, J. P. Thermogravimetric Analysis of the Oxidation of Multiwalled Carbon Nanotubes: Evidence for the Role of Defect Sites in Carbon Nanotube Chemistry. *Nano Lett.* **2002**, *2*, 615–619.
22. Brunauer, S.; Emmett, P. H.; Teller, E. Adsorption of Gases in Multimolecular Layers. *J. Am. Chem. Soc.* **1938**, *60*, 309–319.
23. Inoue, S.; Ichikuni, N.; Suzuki, T.; Uematsu, T.; Kaneko, K. Capillary Condensation of N_2 on Multiwall Carbon Nanotubes. *J. Phys. Chem. B* **1998**, *102*, 4689–4692.
24. Sing, K. S. W. In *Surface Area Determination;* Everett, D. H., Ottewill, R. H., Eds.; Proceedings of the Internation Symposium on Surface Area Determination, 1969; Butterworths: London, 1970; p 25.
25. Peigney, A.; Laurent, Ch.; Flahaut, E.; Bacsa, R. R.; Rousset, A. Specific Surface Area of Carbon Nanotubes and Bundles of Carbon Nanotubes. *Carbon* **2001**, *39*, 507–514.
26. Cassie, A. B. D.; Baxter, S. Wettability of Porous Surfaces. *Trans. Faraday Soc.* **1944**, *40*, 546–551.
27. Barthlott, W.; Neinhuis, C. The Purity of Sacred Lotus or Escape from Contamination in Biological Surfaces. *Planta* **1997**, *202*, 1–8.
28. Windisch, C. F., Jr.; Ferris, K. F.; Exarhos, G. J.; Sharma, S. K. Conducting Spinel Oxide Films with Infrared Transparency. *Thin Solid Films* **2002**, *420*, 89–99.

29. Parker, W. J.; Jenkins, R. J.; Butler, C. P.; Abbott, G. L. Flash Method of Determining Thermal Diffusivity, Heat Capacity, and Thermal Conductivity. *J. Appl. Phys.* **1961**, *32*, 1679–1684.
30. Berber, S.; Kwon, Y. K.; Tomanek, D. Unusually High Thermal Conductivity of Carbon Nanotubes. *Phys. Rev. Lett.* **2000**, *84*, 4613–4616.
31. Hiraoka, T.; Yamada, T.; Hata, K.; Futaba, D. N.; Kurachi, H.; Uemura, S.; Yumura, M.; Iijima, S. Synthesis of Single- and Double-Walled Carbon Nanotube Forests on Conducting Metal Foils. *J. Am. Chem. Soc.* **2006**, *128*, 13338–13339.
32. Fowler, R. H.; Nordheim, L. W. Electron Emission in Intense Electric Fields. *Proc. R. Soc. London, A* **1928**, *119*, 173–181.
33. Bonard, J. M.; Weiss, N.; Kind, H.; Stockli, T.; Forro, L.; Kern, K.; Chatelain, A. Tuning the Field Emission Properties of Patterned Carbon Nanotube Films. *Adv. Mater.* **2001**, *13*, 184–188.
34. Teo, K. B. K.; Chhowalla, M.; Amaratunga, G. A. J.; Milne, W. I.; Pirio, G.; Legagneux, P.; Wyczisk, F.; Pribat, D.; Hasko, D. G. Field Emission from Dense, Sparse, and Patterned Arrays of Carbon Nanofibers. *Appl. Phys. Lett.* **2002**, *80*, 2011–2013.
35. Suh, J. S.; Jeong, K. S.; Lee, J. S.; Han, I. T. Study of the Field-Screening Effect of Highly Ordered Carbon Nanotube Arrays. *Appl. Phys. Lett.* **2002**, *80*, 2392–2394.
36. Futaba, D. N.; Hata, K.; Yamada, T.; Mizuno, K.; Yumura, M.; Iijima, S. Kinetics of Water-Assisted Single-Walled Carbon Nanotube Synthesis Revealed by a Time-Evolution Analysis. *Phys. Rev. Lett.* **2005**, *95*, 056104-1–056104-4.